This article has been accepted for publication in a future issue of this journal, but has not been fully edited. Content may change prior to final publication. Citation information: DOI 10.1109/JESTPE.2020.3045974, IEEE Journal of Emerging and Selected Topics in Power Electronics

Investigation on Amplitude-Domain Modulation for Three-Phase Energy Stored Quasi-Z Source Inverter

Weihua Liang, Yitao Liu, *Senior Member, IEEE,* Runqiu Fang and Jianchun Peng, *Senior Member, IEEE*

***Abstract*—A novel amplitude-domain pulse-width modulation (AD-PWM) technique for three-phase energy stored quasi-Z-source (ES-qZSI) photovoltaic (PV) power system is proposed in this paper. The proposed modulation technique performs switching states and shoot-through behavior based on the relationship of size among three-phase voltages, showing the attractiveness of extreme simplicity and low computation. This paper further investigates the AD-PWM based three-phase PV power system. An active power control method integrated with reactive power compensation for the system in natural coordinate to avoid complicated calculation of trigonometric function. As a result, active power regulation integrated with reactive power compensation is fast and reliable. Compare with the state-of-arts of control schemes for ES-qZSI system utilizing techniques, the proposed control strategy has advantages: 1) The computation is low because there is no shoot-through reference and avoiding complexity vector calculation; 2) there is a reliable capability of ensuring the grid-injected current tracking the grid voltage in phase, owing to the reactive power generated by reactive power equipment is taken into account to control the ES-qZSI's output current. Simulation and experimental results verify the outstanding features of the proposed AD-PWM and active power control strategy integrated with the reactive power compensation technique for three-phase ES-qZSI PV power system.**

***Index Terms*—Quasi-Z-source Inverter, pulse-width modulation, Photovoltaic power system, Reactive power compensator**

I. Introduction

Energy storage quasi-Z-source inverter (ES-qZSI) based photovoltaic (PV) power generation system is quite popular because of its unique features [1-7]: 1) a single-stage inverter topology fulfilling high boost voltage and a continuous current from PV panel; 2) has no dead-time between the upper and lower switches of one bridge leg, and a common ground between DC source and inverter bridge; 3) buffer the fluctuation of PV power, smooth the grid-tie power and store the extra PV power; 4) compensate the power difference between the PV power and the load demand; 5) cope with the wide variation of PV panel voltage. As a result, there has been many researchers working on ES-qZSI/qZSI based PV power system [8-10]. For example, a simple closed-loop control is proposed in [9] to achieve maximum power point tracking (MPPT) of PV panel through Perturb and Observe (P&O), grid power injection control, and energy management strategy for battery safety. In [11], a fixed frequency sliding mode current control method is proposed for a voltage-fed BES-qZSI system.

Output power control, including active and reactive power control, is one of the main tasks, and many methods have been developed [12-19]. For instance, In [12], a control algorithm for grid-tied qZSI PV system with decoupled active and reactive power control is proposed along with energy-loss optimization per switching cycle based on power predictive control (MPC) framework. In [13], an adaptive decoupled power control method is proposed by evaluating the decoupled matrix with the variation ratio of active power and reactive power. In [14], a direct power control method, associated with a space vector modulation DPC-SVM based on super twisting sliding mode control ST-SMC scheme, is proposed. In [15], a reactive current reference algorithm is proposed to enhance the transient performance and minimize the reactive current ripples. In [16], a decoupled active and reactive power control strategy is proposed to address the issue of active and reactive power distribution among cascaded modules in the grid-connected CMI PV power system. In [17], a P-Q decoupled grid-tie power injection is fulfilled with the maximum power capture from PV panels and the unity power factor for ES-qZS inverter-based PV power conversion system. The selective harmonic elimination technique is presented and a decoupled current control method is used to realize reactive power control in [18]. [19] proposes a comprehensive control strategy to achieve PV power generation and reactive power compensation at the same time for the ES-qZS-CHB inverter PV power system. It can be noticed all the aforementioned control schemes are achieved based on the SPWM, SVPWM or SHEPWM. Almost all the existing control schemes are based on the three modulation techniques. Especially, SVPWM is the most applied modulation technique for the three-phase system due to its advantages of high-voltage utilization, low-current harmonics, easy digital implementation with fast processors [20-22]. Therefore, Many modified SVPWM methods are carried for the three-phase qZS/ZS inverter [23-25]. By inserting the shoot-through time into six parts and modifying the six switching times, the ZSSVM6 technique is proposed in [23]. Two

Manuscript received July 23, 2020; revised October 15, 2020; accepted December 15, 2020. This work was supported in part by the Natural Science Foundation of China under Grant 52007122 and in part by the Foundation of Shenzhen Science and Technology Committee under Grant JCYJ20200109105204077. *(Corresponding author: Yitao Liu)*

Weihua Liang is with the College of Mechatronics and Control Engineering, Shenzhen University, Shenzhen 518000, China, and also with the Key Laboratory of Optoelectronic Devices and Systems of Ministry of Education and Guangdong Province, College of Optoelectronic Engineering, Shenzhen University, Shenzhen 518000, China (e-mail: weihualiang@163.com).

Yitao Liu, Runqiu Fang and Jianchun Peng are with the College of Mechatronics and Control Engineering, Shenzhen University, Shenzhen 518000, China (e-mail: liuyt@ieee.org; 849070512@qq.com; jcpeng@szu.edu.cn).

modified space vector modulation strategies were proposed in [24] to reduce the number of switch commutations at the high current level for shorter periods during the fundamental cycle. In the ZSVM2 technique proposed in [25], the total shoot-through time is divided into four realizable parts and modified as two switching times. However, the procedure to implement the SVPWM is complicated due to the difficulty in determining the location of the reference, the calculation of active, zero and shoot-through times in every sector and the determination and selection of the switching states [20]. What's more, the calculations of the coordinate transformation and triangular functions lead to high calculation burden [26-29].

The effort of this paper is to propose a novel and simple modulation for the three-phase ES-qZSI based PV power system to achieve active power control integrated with reactive power compensation, while decreasing calculation burden, speeding up the computations, saving controller resources and lowering system costs. This paper has the following innovative contributions:

1) A novel AD-PWM technique for three-phase ES-qZS inverter is proposed by performing switching states based on the amplitude relationships of size among three-phase voltages and inserting the shoot-through time into a nine-section switching sequence of AD-PWM. The proposed method could avoid shoot-through reference and complexity vector calculation. As a result, the computation time and controller resources would be significantly reduced in practical applications.

2) An active power control integrated with reactive power compensation for the three-phase ES-qZSI PV power system is implemented in natural coordinate-based AD-PWM. By taking the reactive power generated by reactive power equipment into account to control the ES-qZSI's output current, there is a reliable capability of ensuring the grid-injected current tracking the desired reference in phase with the grid voltage.

The rest of this paper are organized as follows: Section II proposes an AD-PWM technique for three-phase ES-qZSI; then, a control strategy of an active power control integrated with reactive power compensation is proposed in Section III; simulation and experimental verifications are shown in Section IV; finally, conclusions of this paper are summarized in Section V.

II. Proposed AD-PWM For Three-phase ES-qZSI

A. Three-phase ES-qZSI

Fig. 1 shows the discussed three-phase ES-qZSI PV power system. The system combines a PV panel, a qZS network, H-bridge inverter, LC filter, grid and AC load. The ES-qZS network includes two inductors L_1 and L_2, two capacitors C_1 and C_2, one switch K_1, one PV panel terminal capacitor C_{in}, and one battery module. The shoot-through state, active state and zero state are fulfilled in continuous conduction mode of each mode, and the equivalent circuits are shown in Fig. 2.

At shoot-through state, the inverter short circuit by turning on the upper and lower switches of any one phase leg at the same time, and qZS diode is turned off because of negative voltage, as shown in Fig. 2 (a). There are (1) where v_{in} denotes the PV panel voltage; v_{C1} and v_{C2} denote the two capacitor voltages; i_{L1} and i_{L2} denote the two inductor currents.

$$\begin{cases} \mathrm{L}_1 \dfrac{di_{\mathrm{L1}}}{dt} = v_{in} + v_{\mathrm{C2}} \\ \mathrm{L}_2 \dfrac{di_{\mathrm{L2}}}{dt} = v_{\mathrm{C1}} \\ \mathrm{C}_1 \dfrac{dv_{\mathrm{C1}}}{dt} = -i_{\mathrm{L2}} \\ \mathrm{C}_2 \dfrac{dv_{\mathrm{C2}}}{dt} = -i_{\mathrm{L1}} + i_{\mathrm{b}} \\ \mathrm{C}_{in} \dfrac{dv_{\mathrm{C}in}}{dt} = i_{pv} - i_{\mathrm{L1}} \end{cases} \tag{1}$$

At non-shoot-through state, the PV panel and qZS inductors charge the qZS capacitors and provide the power to the AC output and the diode is turned on; thus there are

$$\begin{cases} \mathrm{L}_1 \dfrac{di_{\mathrm{L1}}}{dt} = v_{in} - v_{\mathrm{C1}} \\ \mathrm{L}_2 \dfrac{di_{\mathrm{L2}}}{dt} = -v_{\mathrm{C2}} \\ \mathrm{C}_1 \dfrac{dv_{\mathrm{C1}}}{dt} = i_{\mathrm{L1}} - i_{\mathrm{PN}} \\ \mathrm{C}_2 \dfrac{dv_{\mathrm{C2}}}{dt} = i_{\mathrm{L2}} - i_{\mathrm{PN}} + i_{\mathrm{b}} \\ \mathrm{C}_{in} \dfrac{dv_{\mathrm{C}in}}{dt} = i_{pv} - i_{\mathrm{L1}} \end{cases} . \tag{2}$$

When the state space average method is applied to the dynamic equations, the average model of ES-qZSI over switching frequency is (3) where the variables with < > represent the average values over the switching period; D denotes the shoot-through duty ratio.

$$\begin{cases} \mathrm{L}_1 \dfrac{d < i_{\mathrm{L1}} >}{dt} = (\mathrm{D}-1)v_{\mathrm{C1}} + \mathrm{D}\, v_{\mathrm{C2}} + v_{in} \\ \mathrm{L}_2 \dfrac{d < i_{\mathrm{L2}} >}{dt} = \mathrm{D}\, v_{\mathrm{C1}} + (\mathrm{D}-1)v_{\mathrm{C2}} \\ \mathrm{C}_1 \dfrac{d < v_{\mathrm{C1}} >}{dt} = (1-\mathrm{D})i_{\mathrm{L1}} - \mathrm{D}\, i_{\mathrm{L2}} + (\mathrm{D}-1)i_{PN} \\ \mathrm{C}_2 \dfrac{d < v_{\mathrm{C2}} >}{dt} = -\mathrm{D}\, i_{\mathrm{L1}} + (1-\mathrm{D})i_{\mathrm{L2}} + (\mathrm{D}-1)i_{PN} + i_b \\ \mathrm{C}_{in} \dfrac{d < v_{\mathrm{in}} >}{dt} = i_{pv} - i_{\mathrm{L1}} \end{cases} \tag{3}$$

From (3), the inductor currents I_{L1}, I_{L2}, the capacitor voltages V_{C1}, V_{C2}, and DC-link peak voltage V_{PN} can be obtained as

$$\begin{cases} I_{\mathrm{L1}} = \dfrac{D \cdot I_{\mathrm{b}} + (1-D)\cdot I_{\mathrm{PN}}}{1-2D} \\ I_{\mathrm{L2}} = \dfrac{(1-D)\cdot I_{\mathrm{b}} + (1-D)\cdot I_{\mathrm{PN}}}{1-2D} \\ V_{C1} = \dfrac{1-D}{1-2D} V_{in} \\ V_{C2} = \dfrac{D}{1-2D} V_{in} \\ V_{PN} = v_{C1} + v_{C2} = \dfrac{1}{1-2D} V_{in} \end{cases} . \tag{4}$$

This article has been accepted for publication in a future issue of this journal, but has not been fully edited. Content may change prior to final publication. Citation information: DOI 10.1109/JESTPE.2020.3045974, IEEE Journal of Emerging and Selected Topics in Power Electronics

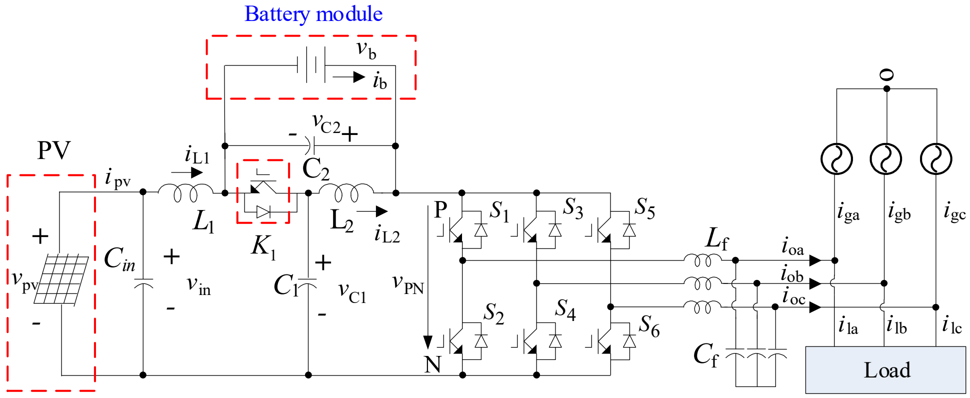

Fig. 1. Discussed three-phase battery energy stored qZSI PV power system.

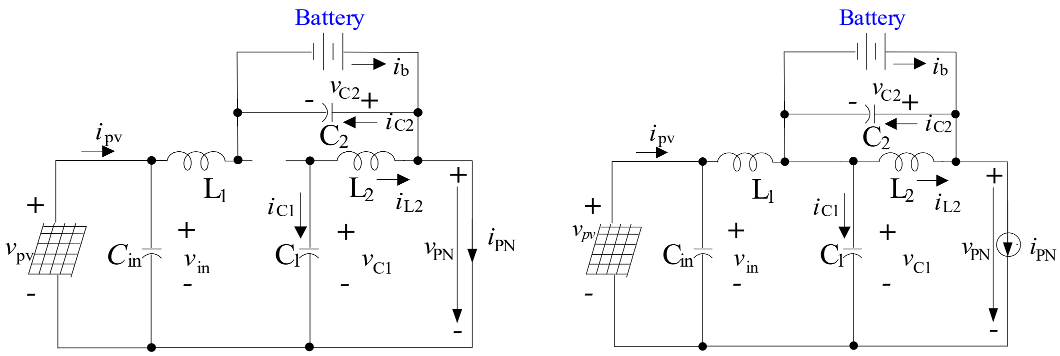

(a) (b)

Fig. 2. Equivalent circuits of BES-qZSI module. (a) Shoot-through state; (b) Non-shoot-through state.

Table I Switching states and the corresponding phase voltage levels

Operating states	S_1	S_2	S_3	S_4	S_5	S_6	Voltage vectors	v_{ao}	v_{bo}	v_{co}
Zero state	0	1	0	1	0	1	U_0	0	0	0
Active state	0	1	0	1	1	0	U_1	$-\frac{1}{3}V_{PN}$	$-\frac{1}{3}V_{PN}$	$\frac{2}{3}V_{PN}$
	0	1	1	0	0	1	U_2	$-\frac{1}{3}V_{PN}$	$\frac{2}{3}V_{PN}$	$-\frac{1}{3}V_{PN}$
	0	1	1	0	1	0	U_3	$-\frac{2}{3}V_{PN}$	$\frac{1}{3}V_{PN}$	$\frac{1}{3}V_{PN}$
	1	0	0	1	0	1	U_4	$\frac{2}{3}V_{PN}$	$-\frac{1}{3}V_{PN}$	$-\frac{1}{3}V_{PN}$
	1	0	0	1	1	0	U_5	$\frac{1}{3}V_{PN}$	$-\frac{2}{3}V_{PN}$	$\frac{1}{3}V_{PN}$
	1	0	1	0	0	1	U_6	$\frac{1}{3}V_{PN}$	$\frac{1}{3}V_{PN}$	$-\frac{2}{3}V_{PN}$
Zero state	1	0	1	0	1	0	U_7	0	0	0
Shoot-through state	1	1	S_3	$\bar{S}_3$	S_5	$\bar{S}_5$	U_8	0	0	0
	S_1	$\bar{S}_1$	1	1	S_5	$\bar{S}_5$	U_9	0	0	0
	S_1	$\bar{S}_1$	S_3	$\bar{S}_3$	1	1	U_{10}	0	0	0

The output voltage of ES-qZSI contains the fundamental-frequency voltage v_i (i=a, b or c) and few high-frequency harmonic voltages. When M is the modulation index, the output peak phase voltage is

$$\hat{v}_i = M \cdot V_{PN} \, . \tag{5}$$

B. Proposed AD-PWM for Three-phase ES-qZSI

The AD-PWM technique is proposed based on the two primary principles:

1) Principle I: taking the reference phase voltage as an average of the nearest voltage levels.

2) Principle II: based on the amplitude relationships among three-phase voltages to select switching states.

1) Switching states and voltage levels

For the three-phase ES-qZSI, there are 11 switching states when only one leg is used to produce the shoot-through state, which includes six active states, two zero state and three shoo-though states. Table I shows the switching states and the corresponding phase voltage levels. There are five voltage levels for each phase, such as -2V_{PN}/3, -V_{PN}/3, 0, V_{PN}/3 and 2V_{PN}/3. The voltage vector U_k (k=0,1,2…10) is a voltage vector group, which denotes different output voltage level for different phase. For example, U_1 denotes -V_{PN}/3 for phases A and B, but denotes 2V_{PN}/3 for phase C. Based on principle I, two active states should be used to generate the desired phase voltage, thereby presenting four states in one switching period: active state1, active state 2, zero state and shoo-through state, and the corresponding switching times are defined as t_1, t_2, t_0 and t_D. According to the volt-second balancing principle, there is

$$\begin{cases} v_{io} = v_1 t_1 + v_2 t_2 + v_0 t_0 + v_D t_D = v_1 t_1 + v_2 t_2 \\ T_s = t_1 + t_2 + t_0 + t_D \\ t_D = DT_s \end{cases} \tag{6}$$

where v_1, v_2, v_0 and v_D denote the phase voltage at active state1, active state 2, zero state and shoo-though state; T_s denotes the switching period.

From (5), (6) and Table I, the times t_1 and t_2 of the active states should satisfy

$$\begin{cases} t_1 \le T_s - t_D = (1-D)T_s \\ t_2 \le T_s - t_D = (1-D)T_s \end{cases}. \tag{7}$$

Then, the average phase voltage meets

$$v_i \in [-\frac{2(1-D)}{3}V_{PN}, \frac{2(1-D)}{3}V_{PN}]. \tag{8}$$

2) *Control sections and switching-state pairs*

The AD-PWM technique is based on the representation of amplitude relationships among three-phase voltages in coordinate axis, and the generated geometry is the control curve clusters shown in Fig. 3, which is a series of elliptic curves. As the voltage amplitude of any one phase is symmetrical about π/2 ± nπ, the amplitude relationships are presented by divided into two parts, as shown in Fig. 3 (b) and (c). From (8), the boundary of control curve clusters is defined by ± (1-D)V_{PN}/2 as the region enclosed by green curves in Fig. 4.

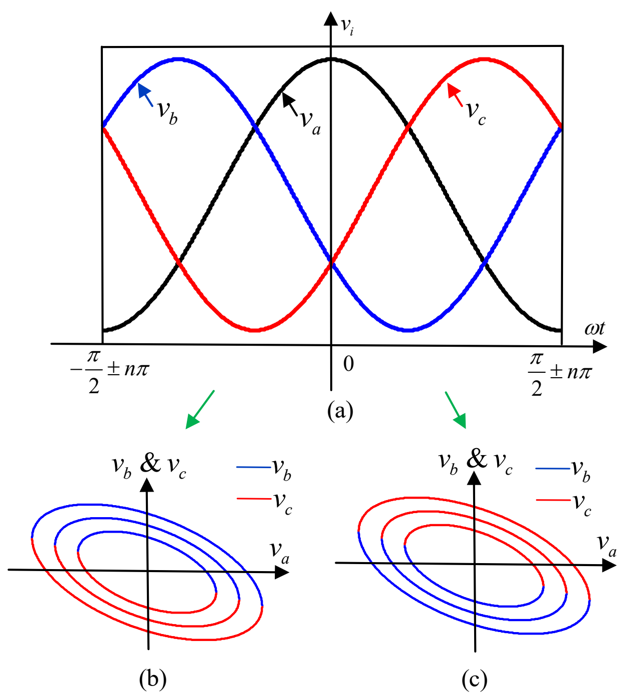

Fig. 3. Amplitude relationships among three-phase voltages;(a) Three-phase voltages;(b) $\omega t \in \left[-\frac{\pi}{2} \pm n\pi, \pm n\pi\right]$; (c) $\omega t \in [\pm n\pi, \frac{\pi}{2} \pm n\pi]$.

According to the voltage value of phase A, and the relationship of voltage amplitudes between phases A and B shown in Fig. 4, switching states and output voltage of phase A can be divided into six sections in the coordinate axis, as shown in Fig. 4 and Table II. Moreover, the operating process to select the operating section is depicted in Fig. 5. From Table I, the voltage vectors and switching pairs, which are used to generate the voltage reference in each section, and can be determined based on the principle I, as shown in Table III.

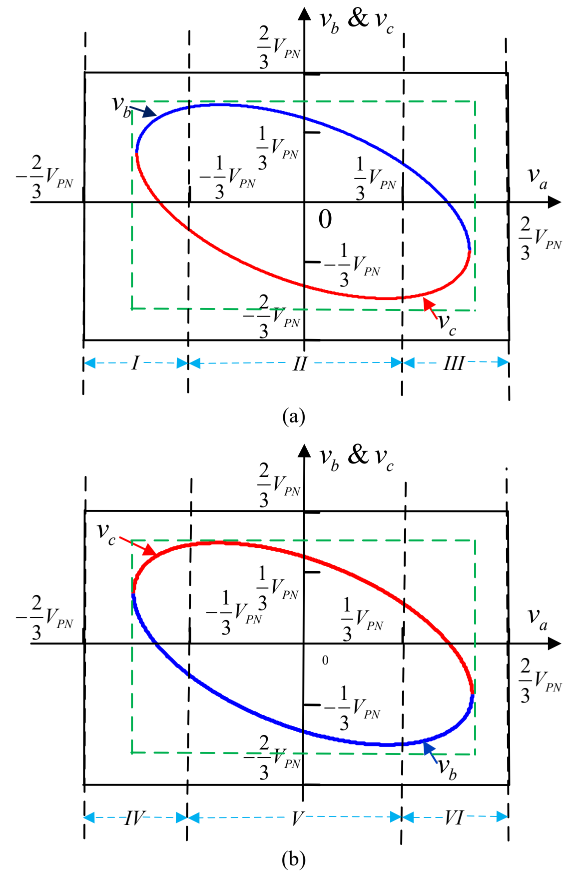

Fig. 4. Boundary of control curve clusters and the corresponding voltage levels; (a) $\omega t \in [-\frac{\pi}{2} \pm n\pi, \pm n\pi]$; (b) $\omega t \in [\pm n\pi, \frac{\pi}{2} \pm n\pi]$

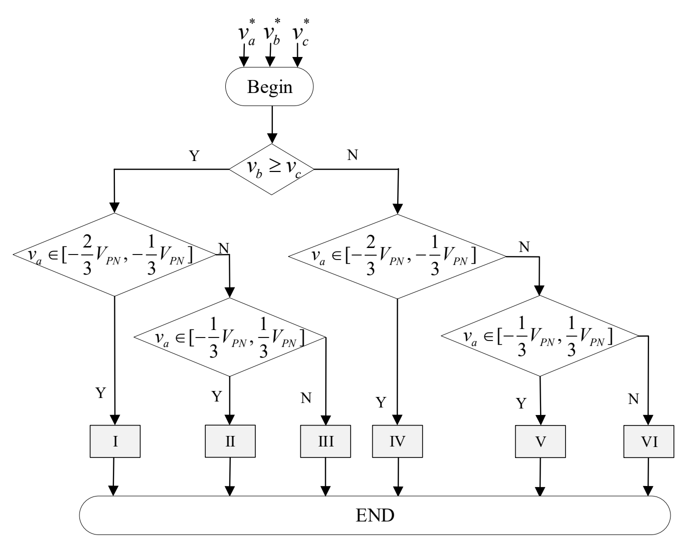

Fig. 5. Flowchart to select the sections

This article has been accepted for publication in a future issue of this journal, but has not been fully edited. Content may change prior to final publication. Citation information: DOI 10.1109/JESTPE.2020.3045974, IEEE Journal of Emerging and Selected Topics in Power Electronics

Table II Trend of phase voltage in each section

Operating Situation		Section
$v_b \geq v_c$	$v_a \in [-\frac{2}{3}V_{PN}, -\frac{1}{3}V_{PN}]$	I
	$v_a \in (-\frac{1}{3}V_{PN}, \frac{1}{3}V_{PN}]$	II
	$v_a \in (\frac{1}{3}V_{PN}, \frac{2}{3}V_{PN}]$	III
$v_b < v_c$	$v_a \in (-\frac{2}{3}V_{PN}, -\frac{1}{3}V_{PN}]$	IV
	$v_a \in (-\frac{1}{3}V_{PN}, \frac{1}{3}V_{PN}]$	V
	$v_a \in (\frac{1}{3}V_{PN}, \frac{2}{3}V_{PN}]$	VI

Table III Voltage vectors and switching pairs used to generate the voltage reference in each section

Section	Voltage Vectors	Switching state pairs of (S_1, S_2, S_3, S_4, S_5, S_6)
I	(U_2, U_3)	(011001), (011010)
II	(U_2, U_6)	(011001), (101001)
III	(U_4, U_6)	(100101), (101001)
IV	(U_1, U_3)	(010110), (011010)
V	(U_1, U_5)	(010110), (100110)
VI	(U_4, U_5)	(100101), (100110)

3) Switching sequence and switching time

Once the section to generate the voltage reference is chosen, the next step is to get the switching time and switching sequence. For a symmetry three-phase system, the sum of three-phase voltages is zero; therefore, the voltage vectors corresponding to the selected section should generate the three-phase voltage references at the same time in each section as

$$\begin{cases} v_{1-a}t_1 + v_{2-a}t_2 = v_a^* \\ v_{1-b}t_1 + v_{2-b}t_2 = v_b^* \\ v_c^* = v_a^* - v_b^* \end{cases} \tag{9}$$

where v_{1-a}, v_{1-b}, v_{2-a} and v_{2-b} denote the vector elements of the selected voltage vector shown in Table III.

From Table I and (9), the switching times can be calculated as

$$\begin{cases} t_D = DT_s \\ t_1 = \dfrac{v_a^* v_{2-b} - v_b^* v_{2-a}}{v_{1-a}v_{2-b} - v_{2-a}v_{1-b}} \\ t_2 = \dfrac{v_a^* v_{1-b} - v_b^* v_{1-a}}{v_{2-a}v_{1-b} - v_{1-a}v_{2-b}} \\ t_0 = T_s - t_D - t_1 - t_2 \end{cases} . \tag{10}$$

The nine-section modulation technique is used to achieve the AD-PWM, as shown in Fig. 6. Table IV shows the sequences of voltage vectors in six sections. Moreover, Fig. 6 and Table IV show the features of the nine-section modulation that each switching period both begins and ends with zero state and shoot-through state inserted between active state and zero state, that would significantly restrain harmonic voltages and reduce switching power loss.

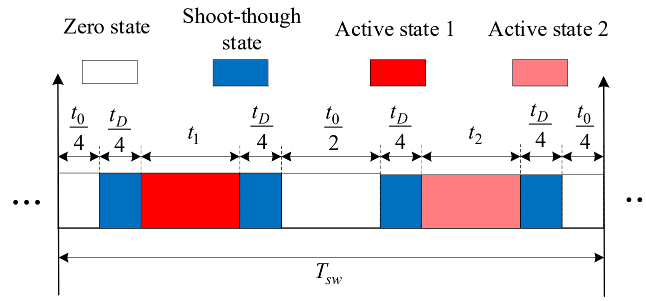

Fig. 6. Switching sequence of AD-PWM technique.

Table IV The sequence of voltage vectors

Section	Sequence of voltage vector
I	$U_0 \to U_9 \to U_2 \to U_{10} \to U_7 \to U_8 \to U_3 \to U_9 \to U_0$
II	$U_7 \to U_{10} \to U_6 \to U_8 \to U_0 \to U_9 \to U_2 \to U_8 \to U_7$
III	$U_0 \to U_8 \to U_4 \to U_9 \to U_7 \to U_{10} \to U_6 \to U_{10} \to U_0$
IV	$U_7 \to U_8 \to U_3 \to U_9 \to U_0 \to U_{10} \to U_1 \to U_8 \to U_7$
V	$U_0 \to U_{10} \to U_1 \to U_8 \to U_7 \to U_9 \to U_5 \to U_{10} \to U_0$
VI	$U_7 \to U_9 \to U_4 \to U_{10} \to U_0 \to U_8 \to U_5 \to U_9 \to U_7$

III. Active Power Control Integrated with Reactive Power Compensation Based AD-PWM For Three-Phase ES-qZSI

The control scheme of the three-phase ES-qZSI based PV power system is shown in Fig. 7, including MPPT control, energy management, calculation of three-phase current in natural coordinate, ES-qZSI's output current control and AD-PWM technique.

As shown in Fig. 7 and [9, 28], PV panel voltage and current are measured, and perturb and observe (P&O) algorithm is used to track the MPP. The shoot-through duty ratio D is adjusted by a PI regulator to make the PV panel voltage track the reference v_{pv}^* and boost PV voltage to a higher level.

A. Energy Management

The goal of energy management is to ensure the state-of-charge (SOC) in safety range that neither be over-charged nor over-discharged, which is achieved by controlling the power difference between ES-qZSI's output power and PV power [30]. The battery will buffer the power difference until SOC reaches its upper/lower safety limitation, then the desired output power is limited to the PV power. The flowchart of implementing energy management is described in Fig. 8, which can be summarized as three cases: 1) when the SOC in safe area as $SOC_{min}<SOC<SOC_{max}$, the ES-qZSI will output power as the given reference P_{oref} and battery will be charged or discharged as needed; 2) when the battery is charged to its SOC upper limitation, battery can be discharged but recharge the battery is prohibited; 3) when the battery is discharged to its SOC lower limitation, discharge the battery is not allowed.

B. Calculation of Three-Phase Currents in Natural Coordinate

Based on instantaneous reactive power theory, the complex power flowing through the ES-qZSI is

$$S = P + jQ = v_i \cdot \bar{i}_i (i = \text{a, b, c}) \tag{11}$$

where $\bar{\iota}_i$ denote conjugate current.

The active power and reactive power can be obtained as (12).

This article has been accepted for publication in a future issue of this journal, but has not been fully edited. Content may change prior to final publication. Citation information: DOI 10.1109/JESTPE.2020.3045974, IEEE Journal of Emerging and Selected Topics in Power Electronics

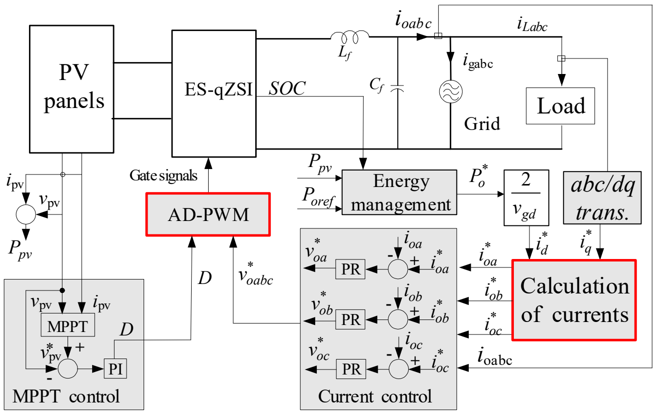

Fig. 7 Control scheme of three-phase ES-qZSI PV power system

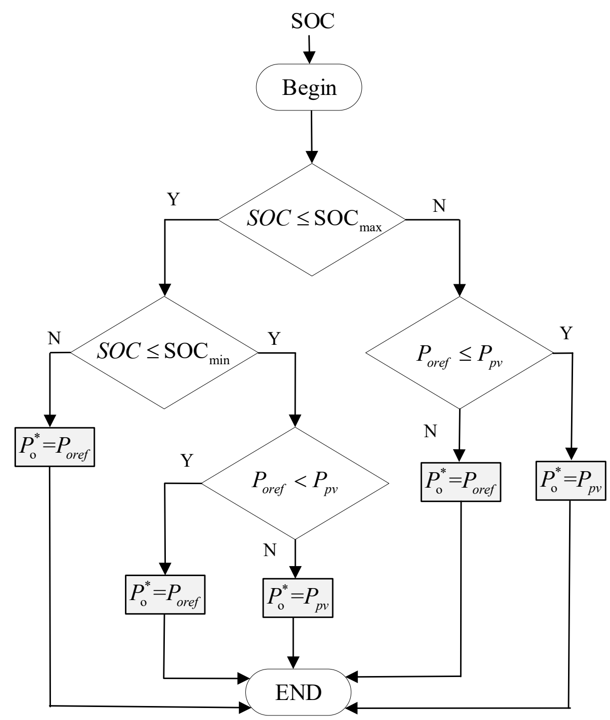

Fig. 8 Flowchart diagram of energy management

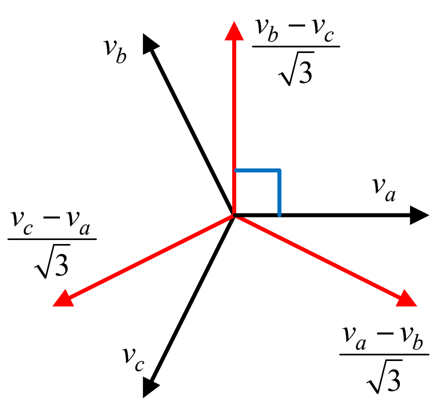
Fig. 9 Three-phase active and reactive vectors

$$\begin{bmatrix} P \\ Q \end{bmatrix} = \begin{bmatrix} v_a & v_b & v_c \\ \frac{v_b - v_c}{\sqrt{3}} & \frac{v_c - v_a}{\sqrt{3}} & \frac{v_a - v_b}{\sqrt{3}} \end{bmatrix} \begin{bmatrix} i_a \\ i_b \\ i_c \end{bmatrix}. \tag{12}$$

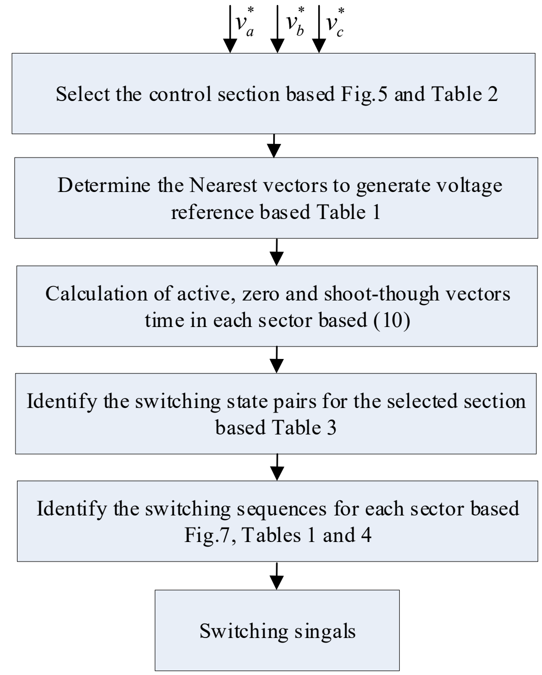

Fig. 10 Flowchart to implement AD-PWM for three-phase ES-qZSI.

From (12), the active power can be viewed as the product of voltage vector and current scalar, and the direction of reactive power is 90 degrees ahead of the voltage vector, as shown in Fig. 9. Therefore, the unit vectors of active power and reactive power are

$$\begin{cases} p_a = \dfrac{v_a}{\sqrt{\frac{2}{3}(v_a^2 + v_b^2 + v_c^2)}} \\ p_b = \dfrac{v_b}{\sqrt{\frac{2}{3}(v_a^2 + v_b^2 + v_c^2)}} \\ p_c = \dfrac{v_c}{\sqrt{\frac{2}{3}(v_a^2 + v_b^2 + v_c^2)}} \end{cases} \tag{13}$$

$$\begin{cases} q_a = \dfrac{p_b - p_c}{\sqrt{3}} \\ q_b = \dfrac{p_c - p_a}{\sqrt{3}} \\ q_c = \dfrac{p_a - p_b}{\sqrt{3}} \end{cases}. \tag{14}$$

From (11)-(14), the desired three-phase currents can be calculated by

$$\begin{cases} i_{oa}^* = \dfrac{i_d^* \cdot p_a + i_q^* \cdot q_a}{3} \\ i_{ob}^* = \dfrac{i_d^* \cdot p_b + i_q^* \cdot q_b}{3} \\ i_{oc}^* = \dfrac{i_d^* \cdot p_c + i_q^* \cdot q_c}{3} \end{cases} \tag{15}$$

where i_d^* and i_q^* are ES-qZSI's desired output active and reactive

This article has been accepted for publication in a future issue of this journal, but has not been fully edited. Content may change prior to final publication. Citation information: DOI 10.1109/JESTPE.2020.3045974, IEEE Journal of Emerging and Selected Topics in Power Electronics

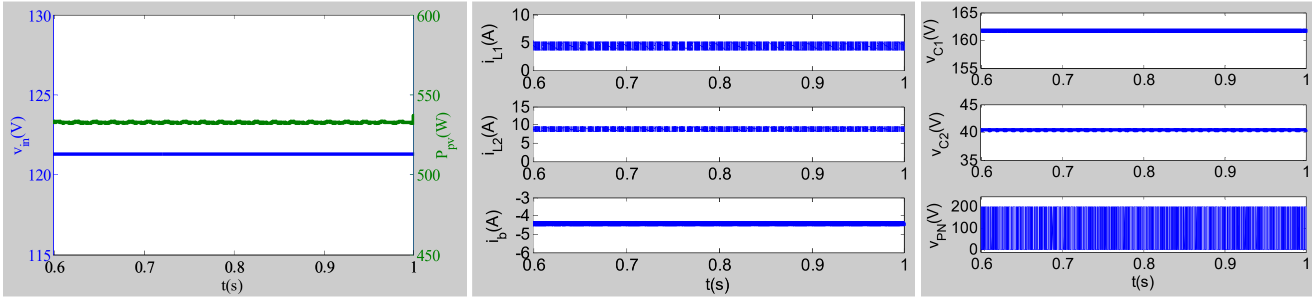

(a) (b) (c)

Fig. 11. Simulation results of ES-qZSI based PV power system with the proposed control method using AD-PWM technique. (a) PV panel's output voltage and power; (b) Inductor currents and battery current; (c) Capacitor voltages and DC-link voltage.

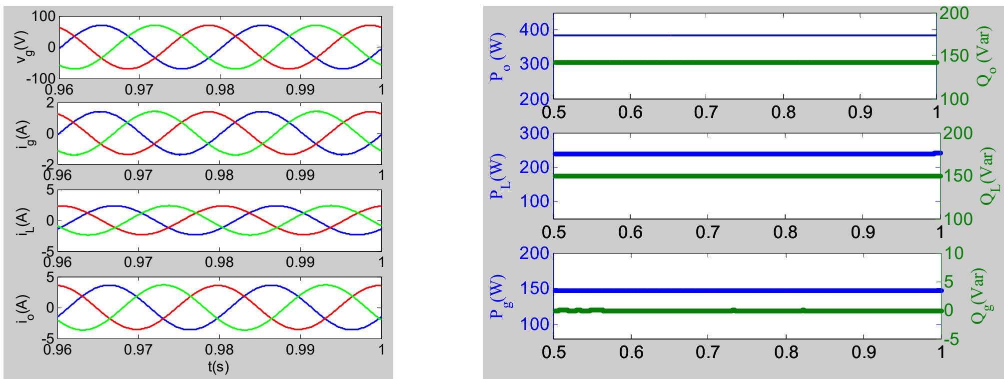

(a) (b)

Fig. 12 Simulation results of ES-qZSI based PV power system with the proposed control method using AD-PWM technique. (a) Grid voltage, grid-injected current, load current and ES-qZSI's output current; (b) ES-qZSIs output power, grid injected power and load power

current, respectively.

As one of the control scheme's goal is to achieve the unity power factor (UPF) grid-connected control, the reactive components of the load current is set as ES-qZSI's desired output reactive current i_q^*, which can be obtained by coordinate transformation, as shown in Fig. 7. The active components of ES-qZSI's desired output current is calculated by

$$i_d^* = \frac{2P_o^*}{3v_{gd}} . \qquad (16)$$

C. ES-qZSI's Output Current Control Based Proposed AD-PWM Technique

The flowchart to implement the AD-PWM technique based on output current control of three-phase ES-qZSI can be described in Fig. 10. ES-qZSI's output voltage references v_{oa}^*, v_{ob}^* and v_{oc}^* are adjusted by PR regulators to make the output current track the reference i_{oa}^*, i_{ob}^* and i_{oc}^* obtained from (15). Then, the control section is identified based on Fig. 4 and Table II. With the switching state pairs, switching times and switching sequences shown in Table III, (10) and Table IV, the gate signals for ES-qZSI are produced to achieve the desired performance.

IV. Simulation and Experimental Investigations

A. Simulation Verification

To verify the proposed AD-PWM technique and control scheme. A prototype of the three-phase BES-qZSI PV power system is built in MATLAB/Simulink. The parameters are: L_1=L_2=1 mH, C_1=C_2=2200 μF, the switching frequency of each module is 10 kHz, the filter is 1.5 mH, and a 50 mH inductor and 25 Ω resistor is connected in series as the local load of each phase, the grid provides 50 V rms voltage through a step down transformer interfaced with ES-qZSI PV power system, and the ES-qZSI's output active power reference is 390 W. The control scheme of Fig. 7 is applied to the system. Simulation with the proposed control method using AD-PWM technique results are shown in Fig. 11.

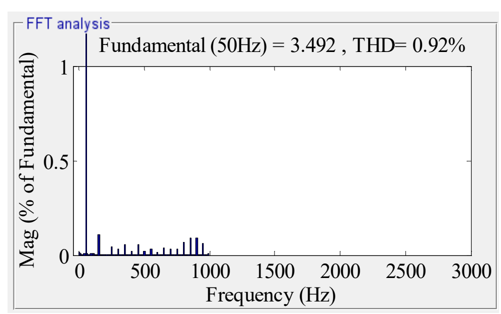

Fig. 13 FFT spectrum of ES-qZSI's output current.

With the proposed control strategy of Fig. 7, the three-phase ES-qZSI based PV power system operates at the MPPs and the PV panel's output voltage and power are v_{pv}=121 V and 533 W, as shown in Fig. 11 (a). The power difference between the PV panel's power and ES-qZSI's output power is buffered by the energy shored batteries with i_b=-4.4 A, as shown in Fig. 11 (b). DC-link pulse voltage shown in Fig. 11 (c) show pulse voltage waveform, because DC-link voltage is zero during the shoot-through state; in the non-shoot-through state, it is non-zero

This article has been accepted for publication in a future issue of this journal, but has not been fully edited. Content may change prior to final publication. Citation information: DOI 10.1109/JESTPE.2020.3045974, IEEE Journal of Emerging and Selected Topics in Power Electronics

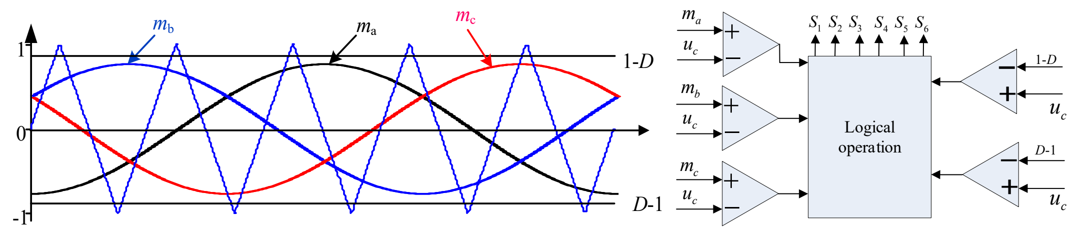

(a) (b)

Fig. 14 SPWM scheme for qZS/ZS inverter. (a) Operating principle; (b) Block diagram.

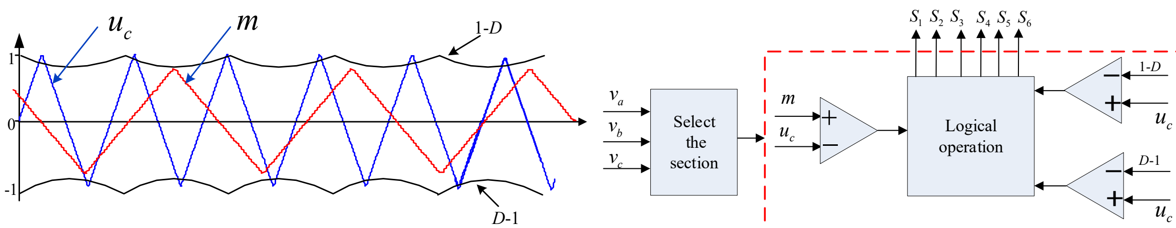

(a) (b)

Fig. 15 PWAM scheme for qZS/ZS inverter. (a) Operating principle; (b) Block diagram.

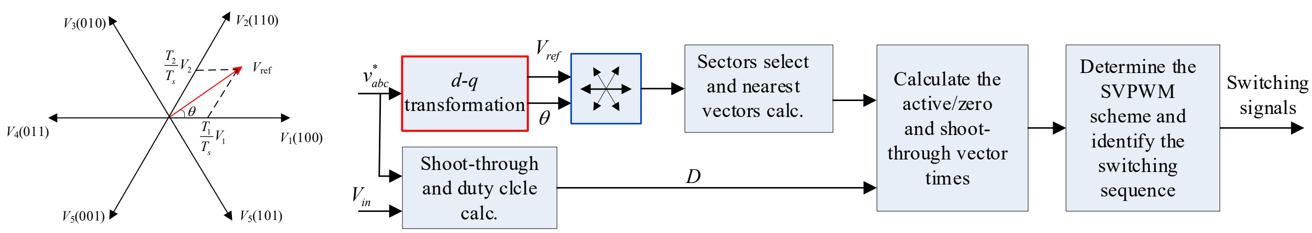

(a) (b)

Fig. 16 SVM scheme for qZS/ZS inverter. (a) Operating principle; (b) Block diagram.

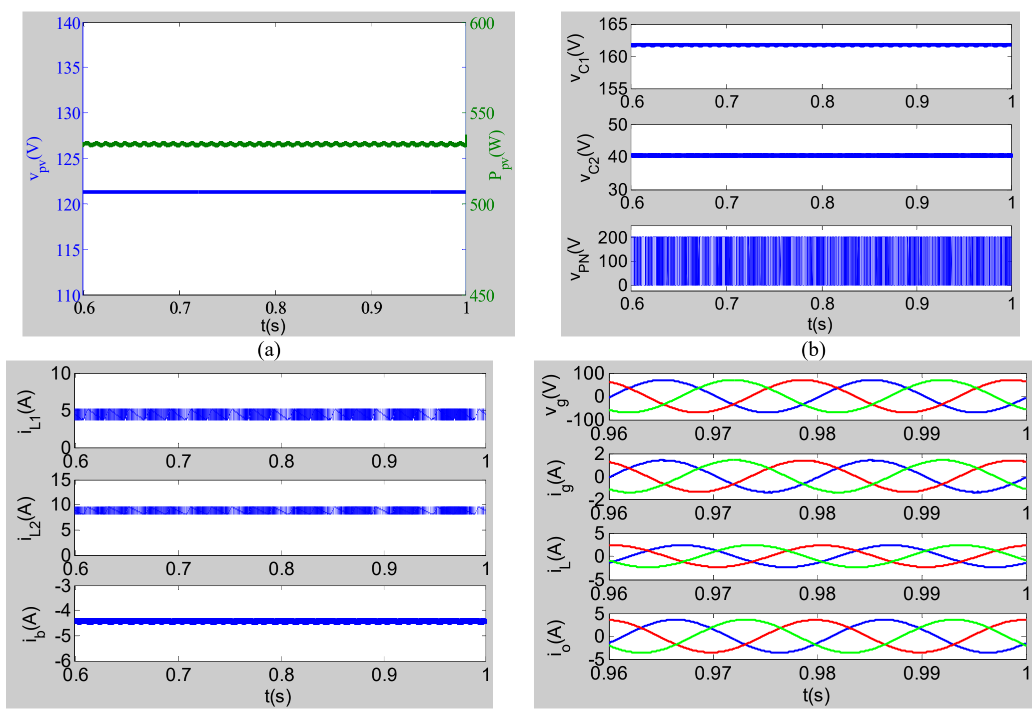

(a) (b) (c) (d)

Fig. 17 Simulation results of ES-qZSI based PV power system with SVM. (a) PV panel's output voltage and power; (b) Capacitor voltages and DC-link voltage; (c) Inductor currents and battery current, (d) Grid voltage, grid-injected current, load current and ES-qZSI's output current.

voltage. Fig. 12 (a) shows the grid voltage, grid-injected current, load current and ES-qZSI's output current. Fig. 12 (b) shows ES-qZSI's output active and reactive power, grid-injected active and reactive power, load active and reactive power. It can be seen that the ES-qZSI's active power is divided into two parts: 150 W of active power provides to the local load and 240

This article has been accepted for publication in a future issue of this journal, but has not been fully edited. Content may change prior to final publication. Citation information: DOI 10.1109/JESTPE.2020.3045974, IEEE Journal of Emerging and Selected Topics in Power Electronics

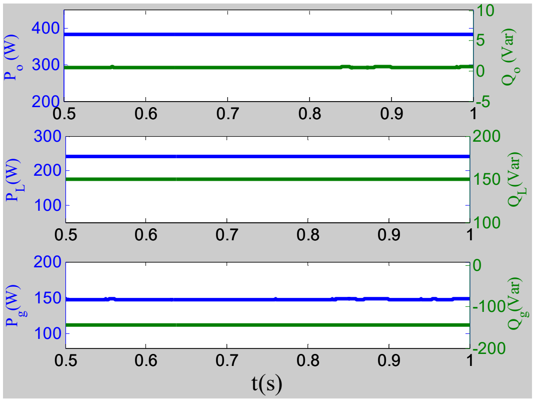

(a)

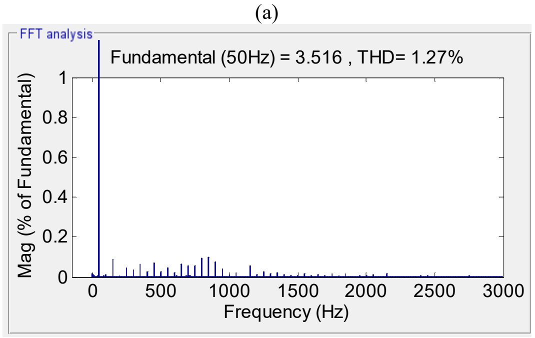

(b)

Fig. 18 Simulation results of ES-qZSI based PV power system with SVM. (a) ES-qZSIs output power, grid injected power and load power; (b) FFT spectrum of ES-qZSI's output current

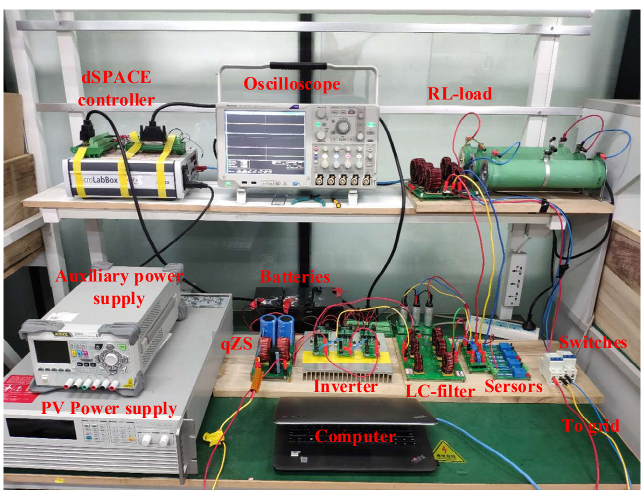

Fig. 19 Experiment set-up of ES-qZS inverter PV power system

W of active power is injected into the grid. However, all the load-reactive power is provided by ES-qZS inverter, and there is no reactive power injected into the grid.

Then, the Fast Fourier Transform (FFT) algorithm is used to analyze the current total harmonic distortion (THD) as shown in Fig. 13. The phase relationships among grid voltage, ES-qZSI's output current and grid-injected current is shown in Table V. From which it can be noted that: 1) with AD-PWM based the proposed control scheme of Fig. 7, the ES-qZSI based PV system presents good performance and the THD of output current is as low as 0.92%; 2) the grid-injected current i_g almost has the same phase with the grid voltage v_g during the whole simulation process, but there is a phase-difference of 16.6° between grid and ES-qZS-CHB's output current, which means the reactive power required by local load is compensated by the ES-qZS-CHB and the system realizes the goal of unity power factor running. All the results above verify the operating principle of AD-PWM based three-phase ES-qZSI and the proposed control strategy.

For comparison, the existing modulation methods such as SPWM [24, 27, 31, 32]. PWAM [33-35], and SVM [17, 22, 23, 27] for the qZS/ZS inverter are summarized in Figs. 14-16. It can be seen that the SPWM and PWAM add two shoot-through references compare with the proposed AD-PWM, in order to compare with the triangular-carrier wave to generate the shoot-through state. In addition, the SVM is realized by voltage vectors composition, which needs higher computation than the other carrier-based modulations. Thus, the proposed method would significantly reduce the computation time, that results in lower the requirement of controller resources in practical applications.

Figs. 17 and 18 show the simulation results of ES-qZS inverter based PV power system using the SVM [17] with the same system parameters. Compare Fig. 12 (a) and Fig. 13 with Fig. 17 (d) and Fig. 18, it can be seen that the proposed AD-PWM enhance the ES-qZSI's output current quality that the THD decreases from 1.27% under SVM to 0.92% under the proposed AD-PWM. Although both methods ensure the reliability and stability of the ES-qZSI based PV power system, as grid voltage, grid-injected current, load current and ES-qZSI's output current shown in Fig. 12 (a) and Fig. 17 (d), the proposed scheme with AD-PWM provides better performance than the scheme with SVM, as the proposed scheme has the reliable capability of ensuring the grid-injected current tracking the desired reference in phase with the grid voltage, as shown in Table V. In addition, the computation of AD-PWM is much less than the SVM.

B. Experimental Verification

A prototype of the three-phase BES-qZSI PV power system is employed to verify the proposed AD-WPM technique and control scheme. Fig. 19 shows the experimental set-up of the ES-qZS inverter PV power system. A CHROMA-62150H-1000 DC power supply is used to simulate a PV power source, auxiliary power supply is a RIGOL-DP832A programmable DC power supply which provides power to control and gate drive boards. The controller is based on dSPACE-MicrolabBox platform to implement the proposed control method. A Tektronix oscilloscope is used to have data and waveforms recorded. Three 12 V/12 Ah batteries of CHAMPION NP12-12 are employed as an energy storage system. The same qZS network parameters (L_1=L_2=1 mH and C_1=C_2=2200 μF) are employed in the experimental test and the switching frequency is 10 kHz. A transformer provides 65 V peak voltage interfaced with the ES-qZSI. The desired ES-qZSI's output power reference is 360 W. The control strategies of Fig. 7 is applied to the system.

Fig. 20 (a) shows the two ES-qZSI's output current, load current, grid-injected current and grid voltage. With the proposed control strategy, ES-qZSI based PV power system operates at the MPPs and the PV panel's output power is 552 W with v_{in}=138 V and i_{L1}=4.0 A, as shown in Fig. 20 (b) and (c). The power difference between the PV panel's power and ES-qZSI's output power is buffered by the energy shored

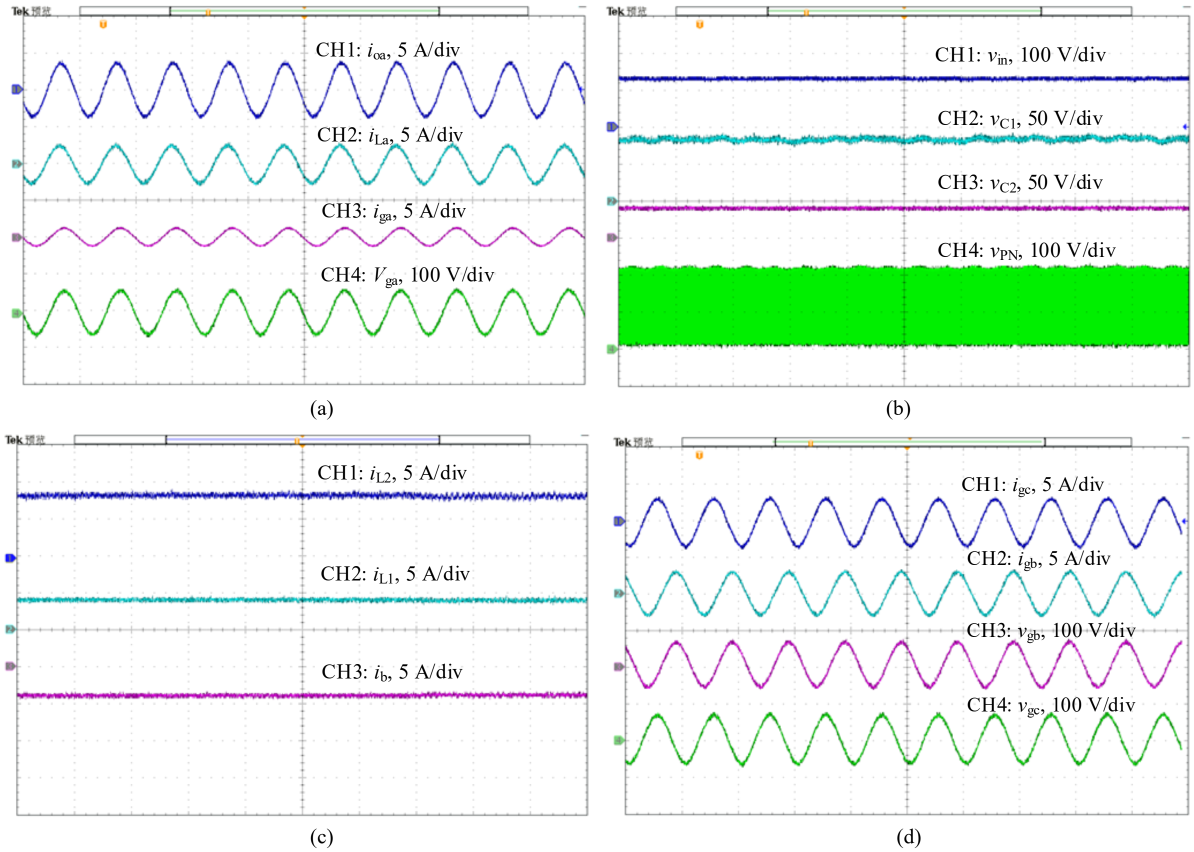

Fig. 20. Experimental results; (a) ES-qZSI's output current, load current, grid-injected current and grid voltage of phase A; (b) PV panel's voltage, capacitor voltages v_{C1}, v_{C2} and DC-link voltage; (c) Inductor voltages i_{L1} and i_{L2} and battery current; (d) Grid-injected currents and voltages of phases B and C.

batteries with i_b=-4.5 A, as shown in Fig. 20 (c).

Fig. 21 shows the FFT spectrum of i_o, and the THD of 1.79% is much lower than 5% with low magnitudes of harmonic components which also meet the requirement of IEEE Std 1547-2018 [36]. Then, the Fast Fourier Transform (FFT) algorithm is used to analyze the current total harmonic distortion (THD) and the phase relationships among grid voltage, ES-qZSI's output current and grid-injected current, and the results are summarized in Table V. It can be noted that: the grid-injected current is purely sinusoidal, and the grid-injected current i_g almost has the same phase with the grid voltage v_g during the whole experimentation process, but there is a phase-difference of 14.5° between grid and ES-qZSI's output current, which means the reactive power needed by local load is compensated by the ES-qZSI and the system realizes the goal of unity power factor running.

Also from Table V, both the simulation-based and experiment-based grid-injected current phases identical to the grid voltage with a little error, although there is a little deviation between the simulation and hardware results, which mainly caused by: 1) the PV panel's MPPs are different in simulation and experiment, as the PV panel's output voltage and power are 121 V and 533 W in simulation, but 138 V and 552 W in the experiment. Moreover, the ES-qZSI's output power are different in simulation (390 W) from that in the experiment (360 W); 2) the experimental grid-voltage is not identical to the simulation grid-voltage performed by an ideal three-phase voltage source; 3) the measurement error and computational error are inevitable in the data measuring and calculating process. All the results above verify the reliable capability of the proposed technique to ensure the grid-injected current tracking the desired reference in phase with the grid voltage.

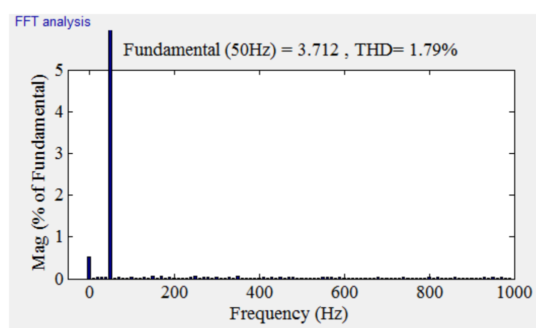

Fig. 21 FFT spectrum of i_o.

Table V Phases difference between grid voltage and grid injected current/ES-qZSI's output current

		$\Delta\varphi_1=\varphi(v_g)-\varphi(i_g)$	$\Delta\varphi_2=\varphi(v_g)-\varphi(i_o)$
Simulation results	FFT results with the proposed scheme using AD-PWM	-0.7°	16.6°
	FFT results with the scheme using SVM [17]	20.3°	-0.9°
Experimental results	FFT results with the proposed scheme using AD-PWM	0.5°	14.5°

V. CONCLUSIONS

In this paper, the AD-PWM technique for the three-phase ES-qZS inverter-based PV power system was proposed. A novel control scheme calculated current reference in natural coordinates to achieve PV power generation and reactive power compensation at the same time by using the AD-PWM technique. By performing switching states and shoot-through behavior based on the relationship of size among three-phase voltages, shoot-through reference and complexity vector calculation are avoided. In addition, as the reactive power generated by reactive power equipment is taken into account to control the ES-qZSI's output current, the proposed control scheme performed a perfect capability of ensuring the grid-injected current tracking the desired reference in phase with the grid voltage, regardless of whether reactive power equipment is connected to the grid-tied ES-qZS inverter. Meanwhile, compared with conventional strategies, the simple calculating process and low computational complexity are the main advantages of the proposed scheme. A test bench based on three-phase ES-qZSI PV power system was built to verify the proposed AD-PWM technique and control strategy. Simulation and experimental results validated the proposed technique.

REFERENCES

[1] Y. Zhang, Q. Liu, J. Li, and M. Sumner, "A Common Ground Switched-Quasi-Z-Source Bidirectional DC–DC Converter With Wide-Voltage-Gain Range for EVs With Hybrid Energy Sources," *IEEE Trans. Ind. Electron.,* vol. 65, no. 6, pp. 5188-5200, Jun. 2017.

[2] H. Cha, Y. Li, and F. Z. Peng, "Practical Layouts and DC-Rail Voltage Clamping Techniques of Z-Source Inverters," *IEEE Trans. Power Electron.,* vol. 31, no. 11, pp. 7471-7479, Nov. 2016.

[3] W. Liang, Y. Liu, B. Ge, X. Li, F. J. T. E. Ferreira, and A. T. d. Almeida, "Night operation, analysis, and control of single-phase quasi-Z-source photovoltaic power system," *IET Renewable Power Gener.,* vol. 13, no. 15, pp. 2817-2829, Nov. 2019.

[4] T. E. Shults, O. Husev, F. Blaabjerg, C. Roncero-Clemente, E. Romero-Cadaval, and D. Vinnikov, "Novel Space Vector Pulsewidth Modulation Strategies for Single-Phase Three-Level NPC Impedance-Source Inverters," *IEEE Trans. Power Electron.,* vol. 34, no. 5, pp. 4820-4830, May. 2019.

[5] S. Sajadian, R. Ahmadi, and H. Zargarzadeh, "Extremum Seeking-Based Model Predictive MPPT for Grid-Tied Z-Source Inverter for Photovoltaic Systems," *IEEE J. Emerging Sel. Top. Power Electron.,* vol. 7, no. 1, pp. 216-227, Mar. 2019.

[6] Y. Shi, T. Kayiranga, Y. Li, and H. Li, "Exploring the LCL Characteristics in GaN-Based Single-L Quasi-Z-Source Grid-Tied Inverters," *IEEE Trans. Ind. Electron.,* vol. 64, no. 10, pp. 7758-7768, Oct. 2017.

[7] M. Meraj, S. Rahman, A. Iqbal, and L. Ben-Brahim, "Common Mode Voltage Reduction in a Single-Phase Quasi Z-Source Inverter for Transformerless Grid-Connected Solar PV Applications," *IEEE J. Emerging Sel. Top. Power Electron.,* vol. 7, no. 2, pp. 1352-1363, Jun. 2019.

[8] B. Ge *et al.*, "An Energy-Stored Quasi-Z-Source Inverter for Application to Photovoltaic Power System," *IEEE Trans. Ind. Electron.,* vol. 60, no. 10, pp. 4468-4481, Oct. 2013.

[9] W. Liang, Y. Liu, and J. Peng, "A Day and Night Operational Quasi-Z Source Multilevel Grid-Tied PV Power System to Achieve Active and Reactive Power Control," *IEEE Trans. Power Electron.,* vol. 36, no. 1, pp. 474-492, Jan. 2021.

[10] D. Sun, B. Ge, W. Liang, H. Abu-Rub, and F. Z. Peng, "An Energy Stored Quasi-Z-Source Cascade Multilevel Inverter-Based Photovoltaic Power Generation System," *IEEE Trans. Ind. Electron.,* vol. 62, no. 9, pp. 5458-5467, Sep. 2015.

[11] J. Liu, S. Jiang, D. Cao, and F. Z. Peng, "A Digital Current Control of Quasi-Z-Source Inverter With Battery," *IEEE Trans. Ind. Inf.,* vol. 9, no. 2, pp. 928-937, May. 2013.

[12] S. Jain, M. B. Shadmand, and R. S. Balog, "Decoupled Active and Reactive Power Predictive Control for PV Applications Using a Grid-Tied Quasi-Z-Source Inverter," *IEEE J. Emerging Sel. Top. Power Electron.,* vol. 6, no. 4, pp. 1769-1782, Dec. 2018.

[13] X. Sun, Y. Tian, and Z. Chen, "Adaptive decoupled power control method for inverter connected DG," *IET Renewable Power Gener.,* vol. 8, no. 2, pp. 171-182, Mar. 2014.

[14] S. Ouchen, M. Benbouzid, F. Blaabjerg, A. Betka, and H. Steinhart, "Direct Power Control of Shunt Active Power Filter using Space Vector Modulation based on Super Twisting Sliding Mode Control," *IEEE J. Emerging Sel. Top. Power Electron.,* to be published, doi: 10.1109/JESTPE.2020.3007900.

[15] L. K. Haw, M. S. A. Dahidah, and H. A. F. Almurib, "A New Reactive Current Reference Algorithm for the STATCOM System Based on Cascaded Multilevel Inverters," *IEEE Trans. Power Electron.,* vol. 30, no. 7, pp. 3577-3588, Jul. 2015.

[16] L. Liu, H. Li, Y. Xue, and W. Liu, "Decoupled Active and Reactive Power Control for Large-Scale Grid-Connected Photovoltaic Systems Using Cascaded Modular Multilevel Converters," *IEEE Trans. Power Electron.,* vol. 30, no. 1, pp. 176-187, Jan. 2015.

[17] Y. Liu, B. Ge, H. Abu-Rub, and F. Z. Peng, "Control System Design of Battery-Assisted Quasi-Z-Source Inverter for Grid-Tie Photovoltaic Power Generation," *IEEE Trans. Sustainable Energy,* vol. 4, no. 4, pp. 994-1001, Oct. 2013.

[18] R. Sajadi, H. Iman-Eini, M. K. Bakhshizadeh, Y. Neyshabouri, and S. Farhangi, "Selective Harmonic Elimination Technique With Control of Capacitive DC-Link Voltages in an Asymmetric Cascaded H-Bridge Inverter for STATCOM Application," *IEEE Trans. Ind. Electron.,* vol. 65, no. 11, pp. 8788-8796, Nov. 2018.

[19] W. Liang, Y. Liu, S. Jiang, J. Peng, and H. Jiang, "Investigation of an STATCOM-based Energy Stored Quasi-Z Source Cascaded H-bridge Inverter Photovoltaic Power System," in *2019 10th International Conference on Power Electronics and ECCE Asia (ICPE 2019 - ECCE Asia)*, *Busan, Korea (South)*, 27-30 May 2019 2019, pp. 1428-1434.

[20] N. Sabeur, S. Mekhilef, and A. Masaoud, "A Simplified Time-Domain Modulation Scheme-Based Maximum Boost Control for Three-Phase Quasi-Z Source Inverters," *IEEE J. Emerging Sel. Top. Power Electron.,* vol. 6, no. 2, pp. 760-769, Jun. 2018.

[21] M. Meraj, S. Rahman, A. Iqbal, and N. A. Emadi, "Novel Level Shifted PWM Technique for Unequal and Equal Power Sharing in Quasi Z Source Cascaded Multilevel Inverter for PV Systems," *IEEE J. Emerging Sel. Top. Power Electron.,* to be published, doi: 10.1109/JESTPE.2019.2952206.

[22] I. Chaib, E. M. Berkouk, J. Gaubert, M. Kermadi, N. Sabeur, and S. Mekhilef, "An Improved Discontinuous Space Vector Modulation for Z-source Inverter with Reduced Power Losses," *IEEE J. Emerging Sel. Top. Power Electron.,* to be published, doi: 10.1109/JESTPE.2020.3002684.

[23] Y. Liu, B. Ge, H. Abu-Rub, and F. Z. Peng, "Overview of Space Vector Modulations for Three-Phase Z-Source/Quasi-Z-Source Inverters," *IEEE Trans. Power Electron.,* vol. 29, no. 4, pp. 2098-2108, Apr. 2014.

[24] A. Abdelhakim, P. Davari, F. Blaabjerg, and P. Mattavelli, "Switching Loss Reduction in the Three-Phase Quasi-Z-Source Inverters Utilizing Modified Space Vector Modulation Strategies," *IEEE Trans. Power Electron.,* vol. 33, no. 5, pp. 4045-4060, May. 2018.

[25] U. S. Ali and V. Kamaraj, "A novel space vector PWM for Z-source inverter," in *2011 1st International Conference on Electrical Energy Systems, Newport Beach, CA, USA*, 3-5 Jan. 2011, pp. 82-85.

[26] J. I. Leon *et al.*, "Multidimensional Modulation Technique for Cascaded Multilevel Converters," *IEEE Trans. Ind. Electron.,* vol. 58, no. 2, pp. 412-420, Feb. 2011.

[27] M. S. Diab, A. A. Elserougi, A. M. Massoud, A. S. Abdel-Khalik, and S. Ahmed, "A Pulsewidth Modulation Technique for High-Voltage Gain Operation of Three-Phase Z-Source Inverters," *IEEE J. Emerging Sel. Top. Power Electron.,* vol. 4, no. 2, pp. 521-533, Jun. 2016.

[28] W. Liang, Y. Liu, B. Ge, and X. Wang, "DC-Link Voltage Balance Control Strategy Based on Multidimensional Modulation Technique for Quasi-Z-Source Cascaded Multilevel Inverter Photovoltaic Power System," *IEEE Trans. Ind. Inf.,* vol. 14, no. 11, pp. 4905-4915, Nov. 2018.

[29] K. Kandasamy, M. Vilathgamuwa, and K. J. Tseng, "Inter-module state-of-charge balancing and fault-tolerant operation of cascaded H-bridge converter using multi-dimensional modulation for electric vehicle application," *IET Power Electron.,* vol. 8, no. 10, pp. 1912-1919, Oct. 2015.

[30] B. Ge, Y. Liu, H. Abu-Rub, and F. Z. Peng, "State-of-Charge Balancing Control for a Battery-Energy-Stored Quasi-Z-Source Cascaded-Multilevel-Inverter-Based Photovoltaic Power System," *IEEE Trans. Ind. Electron.,* vol. 65, no. 3, pp. 2268-2279, Mar. 2018.

This article has been accepted for publication in a future issue of this journal, but has not been fully edited. Content may change prior to final publication. Citation information: DOI 10.1109/JESTPE.2020.3045974, IEEE Journal of Emerging and Selected Topics in Power Electronics

[31] S. P. Sonkar, V. N. Lal, and R. K. Singh, "Three-phase quasi-Z source inverters with regulated multiple AC outputs for microgrid applications and three-phase residential load," *IET Power Electron.,* vol. 13, no. 11, pp. 2222-2235, Aug. 2020.

[32] Y. Zhang *et al.*, "An Improved PWM Strategy for Z-Source Inverter With Maximum Boost Capability and Minimum Switching Frequency," *IEEE Trans. Power Electron.,* vol. 33, no. 1, pp. 606-628, Jan. 2018.

[33] Q. Lei and F. Z. Peng, "Space Vector Pulsewidth Amplitude Modulation for a Buck–Boost Voltage/Current Source Inverter," *IEEE Trans. Power Electron.,* vol. 29, no. 1, pp. 266-274, Jan. 2014.

[34] X. Yu, Q. Lei, and F. Z. Peng, "Boost converter — Inverter system using PWAM for HEV/EV motor drive," in *2012 Twenty-Seventh Annual IEEE Applied Power Electronics Conference and Exposition (APEC)*, *Orlando, FL, USA,* 5-9 Feb. 2012 2012, pp. 946-950.

[35] Y. Liu, B. Ge, H. Abu-Rub, and H. Sun, "Hybrid Pulsewidth Modulated Single-Phase Quasi-Z-Source Grid-Tie Photovoltaic Power System," *IEEE Trans. Ind. Inf.,* vol. 12, no. 2, pp. 621-632, Apr. 2016.

[36] "IEEE Standard for Interconnection and Interoperability of Distributed Energy Resources with Associated Electric Power Systems Interfaces," *IEEE Std 1547-2018 (Revision of IEEE Std 1547-2003),* pp. 1-138, 2018.

Weihua Liang received the B.Sc. degree in electrical engineering from Taiyuan Institute of Technology, Taiyuan, Shanxi, China, in 2012, and the Ph.D. degree in electrical engineering from Beijing Jiaotong University, Beijing, China, in 2018.

From 2018 to 2020, he was a postdoctoral fellow with the College of Mechatronics and Control Engineering, Shenzhen University, Shenzhen, China. He is currently an Assistant Professor with the College of Electrical and Information Engineering, Zhengzhou University of Light Industry, Zhengzhou, Henan, China. His research interests include electrical machine and drive, renewable energy generation, Z-source converter/inverter, etc.

Yitao Liu (S'11-M'15-SM'20) received the B.S. degree in electrical engineering from Wuhan University, Wuhan, China, in 2008, and the M.S. and Ph.D. degrees in electrical and electronic engineering from Nanyang Technological University (NTU), Singapore, in 2009 and 2014, respectively.

From 2014 to 2015, he was a Research Fellow with the Rolls Royce-NTU Joint Laboratory. He is currently an Assistant Professor with the College of Mechatronics and Control Engineering, Shenzhen University, Shenzhen, China. His current research interests include high power density converters, EMI/EMC in power electronics, and wideband-gap devices.

Runqiu Fang received the B. Eng. degree in automation science from Shenzhen university, Shenzhen, China, in 2018. He is currently working toward the M.Eng. degree in control engineering in Shenzhen university, Shenzhen, China.

His research interests include virtual inertia for distributed power system.

Jianchun Peng (M'04–SM'17) received his B.S. and M.S. degrees in Electrical Engineering from Chongqing University, Chongqing, China, in 1986 and 1989, respectively. He received his Ph.D. degree in Electrical Engineering from Hunan University, Hunan, China, in 198l. He was a Visiting Professor from November 2002 to November 2003 with Arizona State University, Tempe, AZ, USA; and from May 2006 to August 2006, with Brunel University, London, ENG, UK.

He is presently working as a Professor at College of Mechatronics and Control Engineering, Shenzhen University, Shenzhen, China. His current research interests include electricity markets, and power system optimal operation and control.